

Effects of periodic scattering potential on Landau quantization and ballistic transport of electrons in graphene

Godfrey Gumbs^{1,2}, Andrii Iurov¹, Danhong Huang³, Paula Fekete⁴ and Liubov Zhemchuzhna⁵

¹ *Department of Physics and Astronomy Hunter College of the City University of New York
695 Park Avenue, New York, NY 10065*

² *Donostia International Physics Center (DIPC), Manuel Lardizabal
4, E-20018, San Sebastian, Basque Country, Spain*

³ *Air Force Research Laboratory,
Space Vehicles Directorate,*

Kirtland Air Force Base, Kirtland, NM

⁴ *West Point Military Academy, West Point, NY*

⁵ *Department of Math and Physics,
NCCU, Durham, NC 27707, USA.*

(Dated: February 27, 2024)

A two-dimensional periodic array of scatterers has been introduced to a single layer of graphene in the presence of an external magnetic field perpendicular to the graphene layer. The eigenvalue equation for such a system has been solved numerically to display the structure of split Landau subbands as functions of both wave number and magnetic flux. The effects of pseudo-spin coupling and Landau subbands mixing by a strong scattering potential have been demonstrated. Additionally, we investigated the square barrier tunneling problem when magnetic field is present, as well as demonstrate the crucial difference in the modulated band structure between graphene and the two-dimensional electron gas. The low-magnetic field regime is particularly interesting for Dirac fermions and has been discussed. Tunneling of Dirac electrons through a magnetic potential barrier has been investigated to complement the reported results on electrostatic potential scattering in the presence of an ambient magnetic field.

PACS numbers: 73.22-f, 73.22 Pr., 71.15.Dx, 71.70.Di, 81.05.U-

Keywords: Hofstadter butterfly, fractal structures, Landau levels, graphene, electron tunneling

Dating back to the early work of Azbel¹ and Hofstadter², the single-particle spectrum of a two-dimensional structure in the presence of both a periodic potential and a uniform ambient perpendicular magnetic field has captivated researchers for many years^{3–19}. The paper by Hofstadter² was for the energy spectrum of a periodic square lattice in the tight-binding approximation and subject to a perpendicular magnetic field. Ever since that time, there have been complementary calculations for the hexagonal lattice³, the two-dimensional electron gas (2DEG) with an electrostatic periodic modulation potential^{10,11,19} and even bilayer graphene where different stacking of the two types of atoms forming the sublattices was considered²⁰. It has been claimed that one may be able to observe evidence of the existence of Hofstadter's butterfly in such experimentally measured quantities as density-of-states and conductivity^{21–23}.

The challenge facing experimentalists so far has been to carry out experiments on 2D structures at achievable magnetic fields where the Hofstadter butterfly spectrum is predicted. One may follow the calculation of Hofstadter by using Harper's equation which may be regarded as a tight-binding approximation of the Schrodinger equation. Then, assuming that the magnetic flux through unit cell of the periodic lattice is a rational fraction p/q of the flux quantum in conjunction with the Bloch condition for the wave function, one obtains a $p \times p$ Hamiltonian matrix to determine the energy eigenvalues since one only needs to solve the problem in a unit cell. Hofstadter himself was concerned about ever reaching magnetic fields where the rich self-similar structure of the butterfly would be experimentally observed due to the estimated high fields required to achieve this.

In this paper, we propose applying an electrostatic modulation potential to a flat sheet of graphene in the presence of a perpendicular magnetic field to produce the energy spectrum with self-similarity at reasonably low magnetic fields. For a review, see¹⁸. We also compare our results with those for a modulated two-dimensional electron gas and discuss the difference. For completeness, we briefly review tunneling of Dirac electrons through a magnetic barrier.

I. MODEL AND THEORY

In the presence of a periodic two-dimensional scattering potential modulation¹⁹

$$V(x, y) = V_0 \left[\cos \left(\frac{2\pi x}{d_x} \right) \cos \left(\frac{2\pi y}{d_y} \right) \right]^{2N}, \quad (1)$$

where $N = 1, 2, \dots$ is an integer, V_0 is the modulation amplitude, and d_x, d_y are the modulation periods in the x and y directions, respectively, we write the Hamiltonian operator as

$$\hat{\mathcal{H}} = v_F \begin{bmatrix} V(x, y) & \hat{p}_x + eB_0 y \hat{x}_0 + i\hat{p}_y & 0 & 0 \\ \hat{p}_x + eB_0 y \hat{x}_0 - i\hat{p}_y & V(x, y) & 0 & 0 \\ 0 & 0 & V(x, y) & \hat{p}_x + eB_0 \hat{x}_0 - i\hat{p}_y \\ 0 & 0 & \hat{p}_x + eB_0 \hat{x}_0 + i\hat{p}_y & V(x, y) \end{bmatrix} \quad (2)$$

$$\hat{\mathcal{H}} = v_F \begin{bmatrix} \hat{\mathcal{H}}_K + V(x, y)\hat{I} & 0 \\ 0 & \hat{\mathcal{H}}_{K'} + V(x, y)\hat{I} \end{bmatrix}. \quad (3)$$

Here, v_F is the Fermi velocity, \hat{I} is a 2×2 identity matrix. In this system, the magnetic flux through unit cell is $\Phi = B_0(d_x d_y)$, which is assumed to be a rational multiple of the flux quantum $\Phi_0 = h/e$, i.e., $\beta \equiv \Phi/\Phi_0 = p/q$ is an irreducible fraction and p and q are integers. Furthermore, we choose the first Brillouin zone defined by $|k_x| \leq \pi/d_x$ and $|k_y| \leq \pi/(q d_y)$. By using the Bloch-Peierls condition, the wave function of this modulated system may be expanded as

$$\Phi_{\ell; n, \vec{k}_{||}}^{\pm}(x, y) = \frac{1}{\sqrt{2\mathcal{N}_y}} \sum_{s=-\infty}^{\infty} \left\{ e^{ik_y \ell_B^2 (sp+\ell) K_1} \times \left[\Psi_{n, k_x - (sp+\ell) K_1}^{K, \pm}(x, y) + \Psi_{n, k_x - (sp+\ell) K_1}^{K', \pm}(x, y) \right] \right\}, \quad (4)$$

where $\vec{k}_{||} = (k_x, k_y)$, $\mathcal{N}_y = L_y/(q d_y)$ is the number of unit cells, which are spanned by $b_1 = (d_x, 0)$ and $b_2 = (0, q d_y)$, in the y direction, $L_y (\rightarrow \infty)$ is the sample length in the y direction, $K_1 = 2\pi/d_x$ is the reciprocal lattice vector in the x direction and $\ell = 1, 2, \dots, p$ is a new quantum number for labeling split p subbands from a k_x -degenerated Landau level in the absence of modulation. The above wave function satisfies the usual Bloch condition, i.e.,

$$\Phi_{\ell; n, \vec{k}_{||}}^{\pm}(x + d_x, y + q d_y) = e^{ik_x d_x} e^{ik_y q d_y} \Phi_{\ell; n, \vec{k}_{||}}^{\pm}(x, y). \quad (5)$$

Since the wave functions at the K and K' points are decoupled from each other for single-layer graphene, which is different from bilayer graphene²⁴, we may write out explicitly the full expression for the wave function at these two points, i.e.,

$$\begin{aligned} \Phi_{\ell; n, \vec{k}_{||}}^{K, \pm}(x, y) &= \frac{C_n}{\sqrt{\mathcal{N}_y L_x}} \sum_{s=-\infty}^{\infty} e^{i[k_x + K - (sp+\ell) K_1]x} e^{ik_y \ell_B^2 (sp+\ell) K_1} \times \\ &\times \begin{bmatrix} \alpha_n^{\pm} \phi_{n-1, k_x + K - (sp+\ell) K_1}(y) \\ \phi_{n, k_x + K - (sp+\ell) K_1}(y) \\ 0 \\ 0 \end{bmatrix}, \end{aligned} \quad (6)$$

$$\begin{aligned} \Phi_{\ell; n, \vec{k}_{||}}^{K', \pm}(x, y) &= \frac{C_n}{\sqrt{\mathcal{N}_y L_x}} \sum_{s=-\infty}^{\infty} e^{ik_y \ell_B^2 (sp+\ell) K_1} \times e^{i[k_x + K' - (sp+\ell) K_1]x} \times \\ &\times \begin{bmatrix} 0 \\ 0 \\ \phi_{n, k_x + K' - (sp+\ell) K_1}(y) \\ \alpha_n^{\pm} \phi_{n-1, k_x + K' - (sp+\ell) K_1}(y) \end{bmatrix}. \end{aligned} \quad (7)$$

From here onwards, we will concentrate on the K point by setting $K = 0$ for convenience and omit the label for the K point thereafter, i.e.,

$$\psi_{\ell,n,\vec{k}_{||}}^{A,\pm}(x,y) \equiv \langle \vec{r}_{||} | \ell, n, \vec{k}_{||}; A, \pm \rangle = \frac{\alpha_n^\pm C_n}{\sqrt{\mathcal{N}_y L_x}} \sum_{s=-\infty}^{\infty} e^{ik_y \ell_B^2 (sp+\ell) K_1} \times e^{i[k_x+K-(sp+\ell)K_1]x} \phi_{n-1, k_x+K-(sp+\ell)K_1}(y) , \quad (8)$$

$$\psi_{\ell,n,\vec{k}_{||}}^{B,\pm}(x,y) \equiv \langle \vec{r}_{||} | \ell, n, \vec{k}_{||}; B, \pm \rangle = \frac{C_n}{\sqrt{\mathcal{N}_y L_x}} \sum_{s=-\infty}^{\infty} e^{ik_y \ell_B^2 (sp+\ell) K_1} \times e^{i[k_x+K-(sp+\ell)K_1]x} \phi_{n, k_x+K-(sp+\ell)K_1}(y) , \quad (9)$$

where $\vec{r}_{||} = (x, y)$. A tedious but straightforward calculation gives rise to an explicit expression for the matrix elements for the potential $V(x, y)$ as

$$V_{\ell,n,\mu}^{\ell',n',\mu'}(\vec{k}_{||}) \equiv \sum_{\vec{k}'_{||}} \int \int dx dy \left[\Phi_{\ell',n',\vec{k}'_{||}}^{\mu'}(x,y) \right]^\dagger V(x,y) \Phi_{\ell,n,\vec{k}_{||}}^\mu(x,y) \quad (10)$$

$$= \frac{V_0 C_{n'} C_n}{4^{2N}} \left\{ e^{ik_y \ell_B^2 K_1 (\ell - \ell')} \sum_{i=0}^{N-1} \sum_{j=0}^{N-1} \left[\mathcal{F}_{ij}^{(B)} + \alpha_{n'}^{\mu'} \alpha_n^\mu \mathcal{F}_{ij}^{(A)} \right] + \delta_{\ell,\ell'} \delta_{n,n'} \left(1 + \alpha_{n'}^{\mu'} \alpha_n^\mu \right) \left[\frac{(2N)!}{(N!)^2} \right]^2 \right\} , \quad (11)$$

where

$$\begin{aligned} \mathcal{F}_{ij}^{(B,A)} &= \binom{2N}{i} \binom{2N}{N} \mathcal{T}_1 + \binom{2N}{j} \binom{2N}{N} \mathcal{T}_2 + 2 \binom{2N}{i} \binom{2N}{j} \mathcal{T}_3 , \\ \mathcal{T}_1 &= A_1^{(B,A)}(0, N-i) , \\ \mathcal{T}_2 &= A_2^{(B,A)}(N-j, 0) , \\ \mathcal{T}_3 &= A_3^{(B,A)}(N-j, N-i) , \end{aligned}$$

as well as the binomial expansion coefficient with $m \geq n$

$$\binom{m}{n} \equiv \frac{m!}{n! (m-n)!} . \quad (12)$$

In the above expressions, we have also introduced the following three self-defined functions

$$A_1^{(B,A)}(r, s) = D_{n',n}^{rs(B,A)} T_\ell^s \delta_{\ell,\ell'} , \quad (13)$$

$$A_2^{(B,A)}(r, s) = D_{n',n}^{rs(B,A)} \left\{ \delta_{\ell-\ell',r} [\text{sgn}(n' - n)]^\xi + \delta_{\ell'-\ell,r} [\text{sgn}(n - n')]^\xi \right\} , \quad (14)$$

$$A_3^{(B,A)}(r, s) = D_{n',n}^{rs(B,A)} \left\{ \delta_{\ell-\ell',r} [\text{sgn}(n' - n)]^\xi \cos[\Theta_{rs}^{\ell'}(n', n)] + \delta_{\ell'-\ell,r} [\text{sgn}(n - n')]^\xi \cos[\Theta_{rs}^\ell(n, n')] \right\} ,$$

where $\xi = |n - n'|$,

$$D_{n',n}^{rs(B)} = \sqrt{\frac{n_1!}{n_2!}} e^{-W_{rs}/(2\beta)} \left(\frac{W_{rs}}{\beta} \right)^{\xi/2} L_{n_1}^{(\xi)} \left(\frac{W_{rs}}{\beta} \right) , \quad (15)$$

$n_1 = \min(n, n')$, $n_2 = \max(n, n')$, $L_n^{(m)}(x)$ is the associated Laguerre polynomial,

$$W_{rs} = \frac{\pi (s^2 K_2^2 + r^2 K_1^2)}{K_1 K_2} , \quad K_2 = \frac{2\pi}{d_y} , \quad D_{n',n}^{rs(A)} = D_{n'-1, n-1}^{rs(B)} , \quad (16)$$

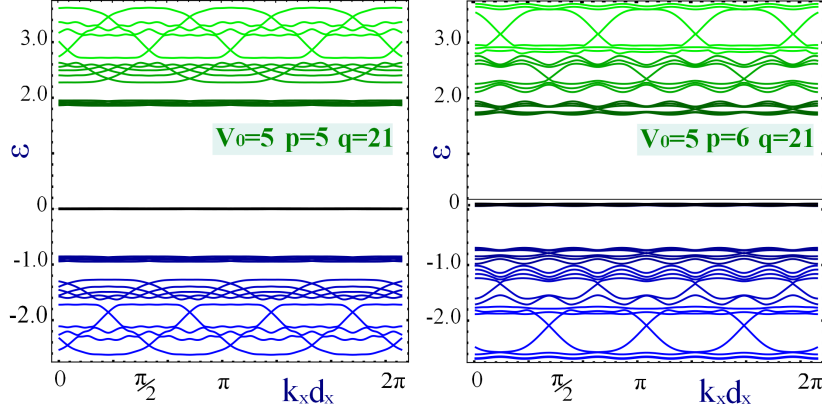


FIG. 1: (Color online). Energy dispersion as functions of $k_x d_x$ for chosen values of V_0 and magnetic flux p/q in units of the flux quantum. The energy is scaled in terms of $v_F \sqrt{eB\hbar}$.

with T_ℓ^s :

$$\begin{aligned} T_\ell^s &= \pm 2 \cos \left[\frac{s(k_x d_x - 2\ell\pi)}{\beta} \right] \delta_{\xi, \{4N, 4N+2\}} , \\ T_\ell^s &= \pm 2 \sin \left[\frac{s(k_x d_x - 2\ell\pi)}{\beta} \right] \delta_{\xi, \{4N+1, 4N+3\}} , \end{aligned} \quad (17)$$

and

$$\Theta_{rs}^\ell(n', n) = \frac{s}{\beta} [k_x d_x - 2\pi(\ell + r/2)] - \text{sgn}(n' - n) \xi \tan^{-1} \left(\frac{s d_x}{r d_y} \right) . \quad (18)$$

The magnetic band structure for this modulated system is a solution of the eigenvector problem $\mathcal{M} \otimes \vec{\mathcal{A}}(\vec{k}_{||}) = 0$ with the coefficient matrix $\vec{\mathcal{M}}$ given by

$$\{\mathcal{M}\}_{j,j'} = \left[E_n^\mu - \varepsilon(\vec{k}_{||}) \right] \delta_{n,n'} \delta_{\ell,\ell'} \delta_{\mu,\mu'}^{(n)} + V_{\ell,n,\mu}^{\ell',n',\mu'}(\vec{k}_{||}) , \quad (19)$$

where $\delta_{\mu,\mu'}^{(n)} = 1$ for $n = 0$ and $\delta_{\mu,\mu'}^{(n)} = \delta_{\mu,\mu'}$ for $n > 0$, $j = \{n, \ell, \mu\}$ is the composite index, and $\{\vec{\mathcal{A}}(\vec{k}_{||})\}_j = \mathcal{A}_{n,\ell}^\mu(\vec{k}_{||})$ is the eigenvector. The eigenvalue $\varepsilon_\nu(\vec{k}_{||})$ of the system is determined by $\text{Det}\{\vec{\mathcal{M}}\} = 0$.

A. Numerical Results for Band Structure

In Fig. 1, we present the dispersion curves as a function of $k_x d_x$ for chosen value of V_0 and two pairs of values of p and q corresponding to two different magnetic field strengths. In each case, there are p Landau subbands, q/p determines the number of oscillation periods in the first Brillouin zone for each of these subbands. Both the valence and conduction subbands are shifted upward but the conduction subbands are shifted more than the valence subbands for each corresponding Landau label for the unmodulated structure. This shift is increased when the modulation amplitude is increased. The original zero-energy Landau level is only slightly broadened and is the least affected by V_0 . If the sign of the modulation amplitude is reversed to correspond to an array of quantum dots, then the subbands are all shifted downward, from their positions for an unmodulated monolayer graphene.

Figure 2 shows the results of our calculations for the energy eigenvalues of modulated graphene as a function of magnetic flux. We included the $n = 0, \pm 1, \pm 2, \pm 3, \pm 4$ as we did in obtaining Fig. 1. For weak magnetic fields, the Landau levels in both valence and conduction bands are slightly broadened into narrow subbands but shifted upward by the perturbing potential V_0 . Another effect due to modulation is to cause these Landau bands to have negative slope at weak magnetic fields which then broaden enough at higher magnetic fields to produce Landau orbit mixing, reflecting the commensurability between the magnetic and lattice Brillouin zones.

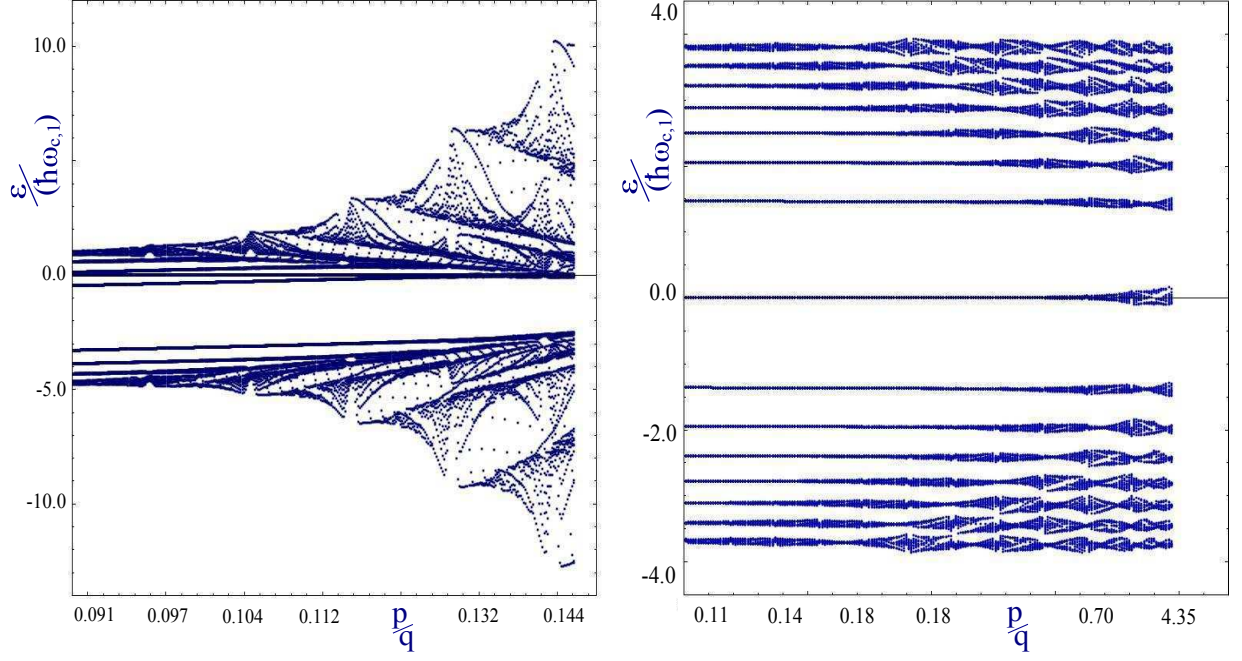


FIG. 2: (Color online). Energy eigenvalues as a function of p/q for graphene for chosen values when $V_0 = 20$ (on the left) and $V_0 = 0.5$ (on the right), $k_x d_x = 0.3$, $k_y d_x = 0.3$. The energy unit is $v_F \sqrt{eB\hbar}$.

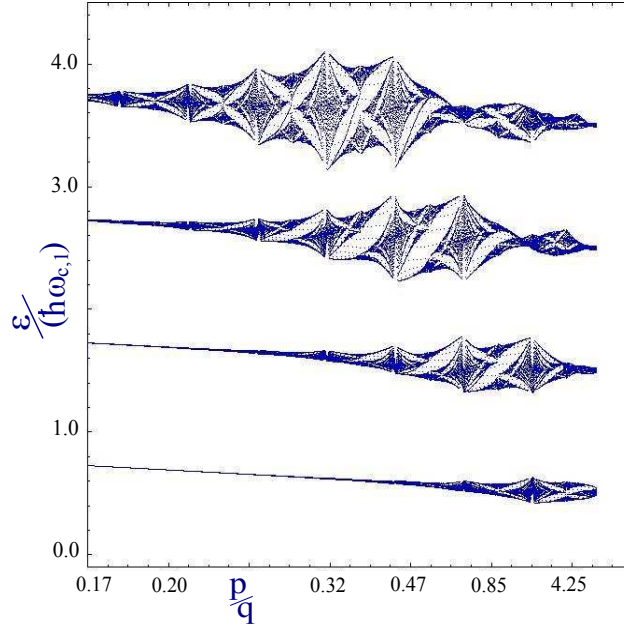


FIG. 3: (Color online). The four lowest Landau subbands for a weakly modulated 2DEG with chosen $V_0 = 0.5$ and $k_x d_x = k_y d_x = 0.3$. The unit of energy is \hbar times the cyclotron frequency.

The lowest perturbed Landau subband which originates from the unperturbed $n = 0$ Landau level merges with the resulting butterfly spectrum at the highest magnetic field compared to the $n = 1, 2, 3, 4$ Landau levels in the conduction band. The onset of the butterfly takes place around $p/q = 1/5$ which would correspond to a magnetic field $B \approx 2$ T for $d_x = d_y = 10$ nm. Furthermore, our calculations have shown that the symmetry between the valence and conduction bands is destroyed by modulation. There is always mixing of the subbands regardless of the value for V_0 . This is in contrast with modulated 2DEG where for weak V_0 , the Landau subbands do not overlap as shown in Fig.

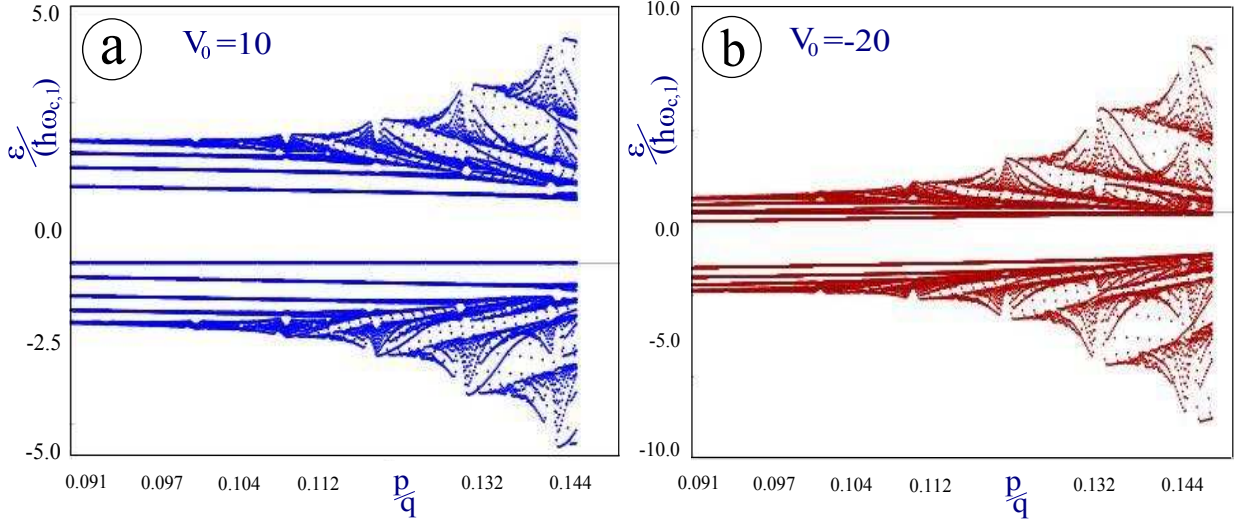


FIG. 4: (Color online). Energy eigenvalues as a function of p/q for graphene. Panel (a) corresponds to $V_0 = 10$ (on the left) and panel (b) - to $V_0 = -20$ (negative potential), $k_x d_x = 0.3$, $k_y d_x = 0.3$. Energy is given in the units is $v_F \sqrt{eB\hbar}$.

3. The lowest subband is shifted upward like the other subbands but is not widened as much as the higher subbands. The feature of self-similarity is also apparent in the excited subbands at intermediate magnetic fields. There is only a shift and broadening of the subbands in the low and high magnetic field regimes for modulated 2DEG.

II. ELECTRON TUNNELING IN THE PRESENCE OF MAGNETIC FIELD

A goal of this paper is to investigate single-particle properties of graphene in the presence of both electric and magnetic fields. Consequently, to complement our derived results in the preceding calculations, we now turn our attention to the standard Klein tunneling problem through a square potential barrier^{25–27} in the presence of the uniform perpendicular magnetic field.

Magnetic barrier and confinement potential for Dirac-Weyl quasiparticles in graphene were addressed in²⁸. The reported results support the result that it is not possible for an electron to tunnel in the presence of a uniform magnetic field. This statement follows from the fact that the two substantially different Landau gauge ($\mathbf{A} = -Bx\hat{e}_y$) and the Symmetric gauge ($\mathbf{A} = \frac{1}{2}\mathbf{B} \times \mathbf{r}$) are expected to result in invariant observables such as current density or electron momentum.

The electrostatic potential barrier is specified by

$$U(x) = U_0 [\theta(w+x) + \theta(w-x) - 1] \quad (20)$$

and the vector potential $\mathbf{A}(x)$ due to the magnetic field $\mathbf{B}(x) = B_0\Theta(d^2 - x^2)\hat{e}_z$ is has the following form

$$\begin{aligned} \mathbf{A}(x) &= A(x)\hat{e}_y, \\ A(x) &= \frac{1}{e\ell_B^2} [-w\theta(w+x) + x\theta(x^2 - d^2) + w\theta(w-x)]. \end{aligned} \quad (21)$$

For this, the eigenvalue equations the spinor wave function with components $\Psi_a(x)$ and $\Psi_b(x)$ and energy ϵ are

$$\begin{aligned} \hbar \left(\frac{\partial}{\partial x} + p_y + eA_y(x) \right) \Psi_b(x) + i U(x) \Psi_a(x) &= i\epsilon \Psi_a(x), \\ \hbar \left(\frac{\partial}{\partial x} - p_y - eA_y(x) \right) \Psi_a(x) + i U(x) \Psi_b(x) &= i\epsilon \Psi_b(x). \end{aligned} \quad (22)$$

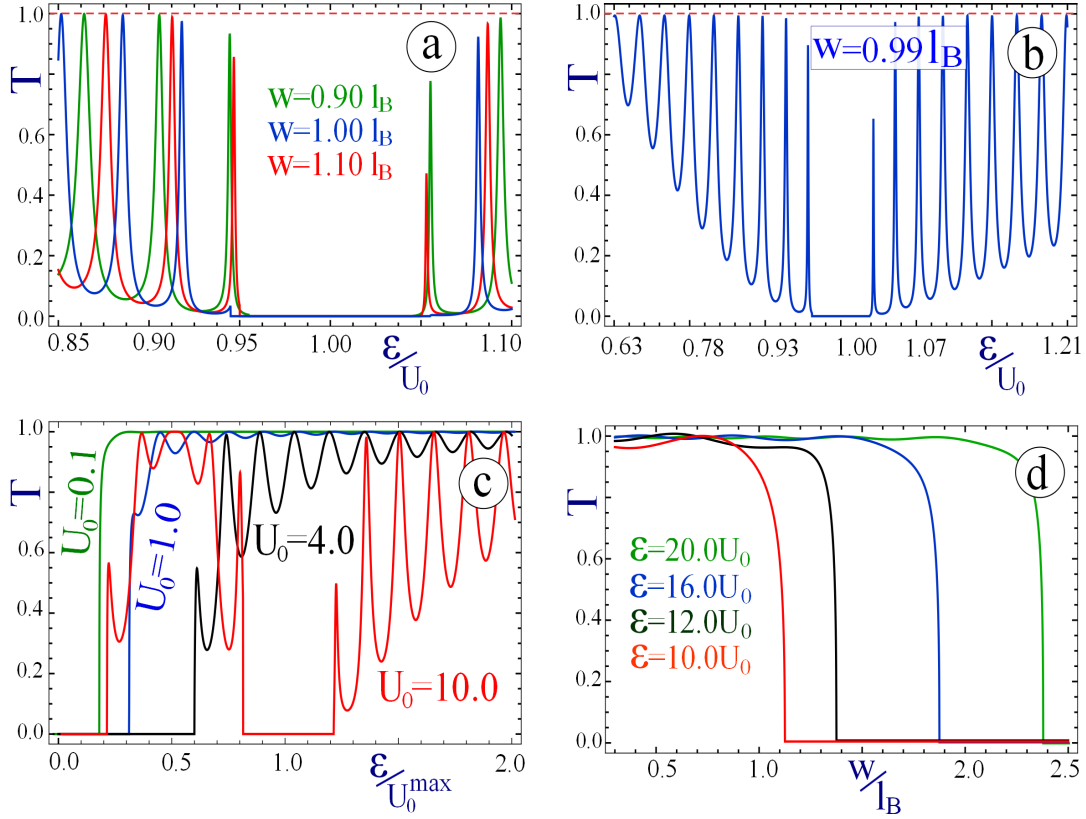


FIG. 5: (Color online). Transmission probability as functions of the incoming electron energy and the barrier width. Panel (a) shows how the transmission depends on the incoming electron energy in the vicinity of the electrostatic barrier height U_0 . The results are provided for chosen values of the barrier width: $w/\ell_B = 0.9, 1.0, 1.1$. Panel (b) presents results for $w/\ell_B = 0.99$ and a wider range of energy. Panel (c) shows the energy dependence of transmission for various barrier heights U_0 , with one of them in the vicinity of zero. The energies are plotted in the units of the largest barrier height U_0^{max} . Plot (d) shows the transmission probability as a function of barrier width for chosen values of the incoming particle energy $\epsilon/U_0 = 20, 16, 12$ and 10 .

where $U(x) = U_0$ is the electrostatic potential in the barrier region.

First, we notice that due to the specific spatial dependence of the potentials for both $\mathbf{A}(x)$ and $V(x)$, the transverse component of the electron momentum is conserved. This leads to the form of the electron wave function in each region. The system [22], determining the wave function components results in the following equations:

$$\hbar^2 \frac{d^2 \psi_{a/b}(x)}{dx^2} - \left(\pm e \frac{dA(x)}{dx} + (\hbar k_y + eA(x)) \right) \psi_{a/b}(x) = (\epsilon - U(x))^2 \psi_{a/b}(x). \quad (23)$$

In the barrier region, this equation has solutions in the form of parabolic cylinder functions. The incoming particle, incident at angle ϕ with the normal to the barrier, has wave function on the left of the barrier given by

$$\Psi_{in}(x) = \frac{1}{\sqrt{2}} \left(\frac{1}{p_x + i(p_y - \hbar d/\ell_B^2)} \right) e^{i\hbar p_x x}, \quad (24)$$

where $p_x = \epsilon \cos \phi$, $p_y = \epsilon \sin \phi + \hbar d/\ell_B^2$ and $\mathbf{s} = [\epsilon - U(x)]$. The solution within the barrier region is given as follows

$$\Psi_b(x) = \mathcal{N} \left(\frac{\mathcal{D}_{\eta-1}(\pm\sqrt{2}\zeta)}{\mathbf{s}\sqrt{1/\eta} \mathcal{D}_{\eta}(\pm\sqrt{2}\zeta)} \right) e^{i\hbar p_x x} \quad (25)$$

with $\zeta = x/\ell_B + p_y \ell_B$ and $\eta = ((\epsilon - U(x))\ell_B)^2/2$.

In contrast to the electrostatic potential barrier, the magnetic barrier leads to confinement of Dirac electrons in graphene. In agreement with²⁸, we find that for chosen incoming energy and angle of incidence, there is a maximum width of the barrier for finite transmission probability. When we also include an electrostatic potential barrier and

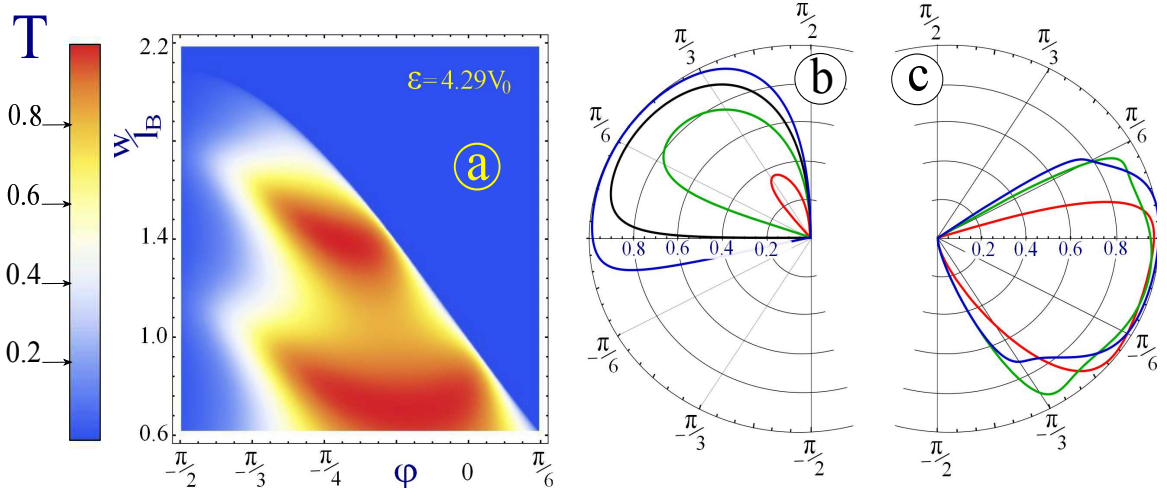


FIG. 6: (Color online). Angular dependence of the electron transmission. Panel (a) is a density plot of the transmission probability as a function of both incoming energy and the angle of incidence. Panels (b) and (c) present polar plots of electron transmission. The results in panel (b) are shown for chosen values of the incoming energy ($\epsilon/U_0 = 3.75, 5.00, 6.25$ and 7.5) and in panel (c) for chosen barrier width values ($w/\ell_B = 1.2, 1.3$ and 1.4).

take into account electron-hole transition, the energy is renormalized in the barrier region and may be arbitrarily small, which makes the tunneling impossible even for low-width barriers. However, for the case when $U_0 \gg \epsilon$, the transmission probability is restored and may be equal or close to unity, depending on the barrier width. As far as the angular dependence of the transmission is concerned, the largest tunneling probability does not correspond to head-on collision ($\phi = 0$), but at a finite angle of incidence, revealing the asymmetry due to the applied magnetic field. A sharp drop in the transmission coefficient close to the critical thickness of the barrier corresponds in the classical limit to circular trajectories of the electrons.

The transmission coefficient is obtained by matching the wave function at the boundary of each region, keeping in mind that the longitudinal momentum does not remain constant in the barrier region, i.e.,

$$T = \frac{p_{x,3}}{p_{x,1}} |t|^2, \quad (26)$$

$$T = \frac{\sqrt{2}e^{-i\hbar w(p_{x,1}+p_{x,3})} (1 + e^{2i\phi}) \ell_B (\epsilon - U_0) \{ \Lambda^{2,+} \Xi^{2,+} + \Lambda^{2,-} \Xi^{2,+} \}}{2i e^{i\phi} \Upsilon_1 + i e^{i\phi_2} (U_0 - \epsilon) \epsilon \Upsilon_2 + \sqrt{2} e^{i(\phi+\phi_2)} \epsilon \Upsilon_3 - \sqrt{2} (U_0 - \epsilon) \Upsilon_4}.$$

In this notation, $\Upsilon_1 = \Xi^{1,+} \Lambda^{2,-} - \Xi^{1,+} \Lambda^{2,-}$, $\Upsilon_2 = \Lambda^{1,+} \Lambda^{2,-} - \Lambda^{1,-} \Lambda^{2,+}$, $\Upsilon_3 = \Lambda^{1,+} \Xi^{2,-} + \Lambda^{2,+} \Xi^{2,+}$, $\Upsilon_4 = \Lambda^{2,+} \Xi^{1,-} + \Xi^{2,-} \Lambda^{1,+}$ and

$$\begin{aligned} \Lambda^{1,\pm}(\epsilon, U_0, \phi, w) &= \mathcal{D}_{\eta-1}(\pm\sqrt{2}(-\frac{w}{\ell_B} + p_y \ell_B/\hbar)), \\ \Xi^{1,\pm}(\epsilon, U_0, \phi, w) &= \mathcal{D}_{\eta}(\pm\sqrt{2}(-\frac{w}{\ell_B} + p_y \ell_B/\hbar)), \\ \Lambda^{2,\pm}(\epsilon, U_0, \phi, w) &= \mathcal{D}_{\eta-1}(\pm\sqrt{2}(\frac{w}{\ell_B} + p_y \ell_B/\hbar)), \\ \Xi^{2,\pm}(\epsilon, U_0, \phi, w) &= \mathcal{D}_{\eta}(\pm\sqrt{2}(\frac{w}{\ell_B} + p_y \ell_B/\hbar)). \end{aligned} \quad (27)$$

Numerical results for electron transmission are presented in Fig.[5] and Fig.[6]. Our general conclusion is that the transmission incorporates properties of both electric and magnetic potential barriers. Equivalent transmission resonances may be observed for $\epsilon < U_0$, which corresponds to electron-hole transition at the boundary of the potential region.

We note that the *electrostatic potential* U_0 increases and drops sharply at the boundaries, whereas the *magnetic vector potential* is continuous. However the electrostatic potential is uniform inside the barrier region. This significant difference in the spatial dependence suggests that we may consider the effect due to each potential separately as an adequate approximation. As a matter of fact, we take into account the refraction due to the electrostatic potential

barrier first, and then deal with the transmission of the new state in the magnetic barrier. Consequently, the *energy - width* relationship, determining the condition of complete reflection, must now include the energy in the barrier region $\epsilon - U_0$. As a result, the transmission drops to zero in the vicinity of $\epsilon = U_0$, as we can clearly see from Fig.[4].

We define the transmission resonances as asymmetric the peaks of the transmission for both electron and hole states in the barrier region. The term comes from the theory of the *Klein paradox* and is employed to separate the head-on complete transmission with its peaks corresponding to the different angles of incidence. In contrast to the Klein paradox which persists for the barriers of arbitrary width and height, the resonances occur for different angles of incidence and the particle energies which depend on the above mentioned parameters. As far as the transmission resonances in the presence of magnetic field are concerned, they exhibit similar properties to the case of pure electric barrier.

We also conclude that the transmission resonances disappear in the limit when $U_0 \rightarrow 0$, i.e., when only the magnetic barrier is present. It is interesting to note that even for a finite value of U_0 , there are no peaks for $\epsilon < U_0$. It could be explained by the fact that for incoming particle energies close to the barrier height, the transmission is suppressed. Analyzing the transmission probability dependence on the barrier width, we confirm that there exists a critical width w_{cr} , such that for any barrier whose width exceeds this critical value, the transmission is completely suppressed. This corresponds to a sharp drop of transmission next to the critical value of the barrier width. This critical value decreases with increasing electron energy. For $w < w_{cr}$, the transmission exhibits peaks and somewhat oscillatory but not periodic behavior.

Angular dependence of the electron transmission probability, presented in Fig.[5], also demonstrates several interesting features. The transmission maximum no longer corresponds to head-on collision, but is shifted to a finite angle which is determined by the incoming electron energy. Transmission dependence shows the decrease with drastically different properties, corresponding to the larger and smaller angles compared to the angle with the largest transmission probability. For a larger angle of incidence, the decrease is moderate. However, in the opposite direction, we observe a sharp drop. For the barrier width dependence, we once again see oscillatory behavior (see the density plot, panel (a) of Fig.[5]). There are also angular transmission resonances present.

III. CONCLUDING REMARKS

In this paper, we Presented a formalism for calculating the energy band structure for an electrostatically modulated single-layer of graphene in the presence of a uniform perpendicular magnetic field. At low and high magnetic fields, the Landau levels are broadened into non-overlapping minibands. However, at intermediate fields, the commensurability relations between the modulation period and the cyclotron radius cause a mixing of the Landau orbits and overlapping of the subbands. The resulting picture is that of a Hofstadter butterfly for the conduction and valence bands. The onset of the self-similarity in the energy band structure depends on the modulation amplitude. The minibands for graphene always overlap in the presence of an electrostatic modulation, unlike the 2DEG. We also obtained the energy dispersion for graphene. The asymmetry of these curves in the valence and conduction subbands is due to modulation as may be seen from our eigenvalue equation $\text{Det}\{\vec{\mathcal{M}}\} = 0$ where the matrix $\vec{\mathcal{M}}$ is defined in Eq. (19).

Also, we addressed the electron tunneling problem in the presence of both electrostatic and magnetic potential barriers within the same region. We have found that transmission is suppressed for incoming electron energies close to the barrier height and for barrier widths exceeding critical values. In contrast, transmission resonances exist for the case of electron-hole transmission at the boundary of the potential region. The angular dependence of the electron transmission probability demonstrates the shift of the transmission maximum to a finite angle of incidence, compared to Klein paradox for purely electrostatic potential barriers.

Acknowledgments

This research was supported by contract # FA 9453-07-C-0207 of AFRL.

¹ M. Ya. Azbel, Sov. Phys. JETP, **19**, 634 (1964).

² D. R. Hofstadter, Phys. Rev.B **14**, 2239 (1976).

³ Godfrey Gumbs and Paula Fekete, Phys. Rev. B **56**, 3787 (1997).

⁴ G. H. Wannier, Phys. Stat. Sol. b **100**, 163 (1980).

⁵ A. Rauh, G. H. Wannier, and G. Obermair, Phys. Stat. Solidi b **63**, 215 (1974).

- ⁶ A. Rauh, Phys. Stat. Sol. b **69**, K9 (1975).
- ⁷ H. W. Neumann and A. Rauh, Phys. Stat. Solidi b **96**, 233 (1979).
- ⁸ Y. Hasegawa, Y. Hatsugai, M. Kohmoto, and G. Montambaux, Phys. Rev. B **41**, 9174 (1990).
- ⁹ Y. Hatsugai and M. Kohmoto, Phys. Rev. B **42**, 8282 (1990).
- ¹⁰ D. Pfannkuche and R. R. Gerhardts, Phys. Rev. B **46**, 12606 (1992).
- ¹¹ D. Pfannkuche and R. R. Gerhardts, Surf. Sci. **263**, 324 (1992).
- ¹² D. J. Thouless, Phys. Rev. B **28**, 4272 (1983).
- ¹³ F. Claro, Phys. Stat. Sol. (b) **104**, K31 (1981).
- ¹⁴ H. J. Schellnhuber and G. M. Obermair, Phys. Rev. Lett. **45**, 276 (1980).
- ¹⁵ T. Perschel and T. Geisel, Phys. Rev. Lett. **71**, 239 (1993).
- ¹⁶ X. Wu and S. E. Ulloa, Phys. Rev. B **47**, 10028 (1993).
- ¹⁷ H. Silbernauer, J. Phys.: Condens. Matter **4**, 7355 (1992).
- ¹⁸ J. B. Sokoloff, Physics Reports **126**, 189 (1985).
- ¹⁹ O. Kühn, V. Fessatidis, H. L. Cui, P. E. Selbmann, and N. Horing, Phys. Rev. B **47**, 19, 13019 (1993).
- ²⁰ N. Nemeć and G. Cunibert, Phys. Rev. B **75**, 201404(R) (2007).
- ²¹ P. D. Ye, D. Weiss, R. R. Gerhardts, M. Seeger, K. von Klitzing, K. Eberl, and H. Nickel, Phys. Rev. Lett. **74**, 3013 (1995).
- ²² C. R. Dean et al., Nature **497**, 598 - 602 (30 May 2013).
- ²³ L. A. Ponomarenko et al., Nature **497**, 594 - 597 (30 May 2013).
- ²⁴ M. Zarenia, P. Vasilopoulos, and F. M. Peeters, Phys. Rev. B, **85**, 245426 (2012).
- ²⁵ M. I. Katsnelson, K. S. Novoselov, and A. K. Geim, Nature Physics, **2**, 620 (2006).
- ²⁶ Andrii Iurov, Godfrey Gumbs, Oleksiy Roslyak and Danhong Huang, Journal of Physics.: Condensed Matter, **24**, 1, 015303 (2012)
- ²⁷ Andrii Iurov, Godfrey Gumbs, Oleksiy Roslyak and Danhong Huang, Journal of Physics.: Condensed Matter, **25**, 13, 135502 (2013)
- ²⁸ A. De Martino, L. Dell'Anna and R. Egger, Solid State Communications, **144**, 12 (2007).